Polarization of light scattered by microrough surfaces and subsurface defects

Thomas A. Germer and Clara C. Asmail

Optical Technology Division

National Institute of Standards and Technology

Gaithersburg, Maryland 20899

ABSTRACT

The polarization of light scattered into directions out of the plane of incidence for 532 nm light incident at 45° with p-polarization was measured from rough silicon, rough titanium nitride, polished fused silica and glass ceramic, and ground and incompletely polished black glass. Models for polarized light scattering from microroughness, subsurface defects, and facets are reviewed. The measurements demonstrate the validity of the models and the utility of polarized light scattering measurements for distinguishing between roughness and defects.

1. INTRODUCTION

The amount of light scattered by a material is often a sensitive measure of the quality of that material.[1] Since a perfectly smooth surface of a material having translational symmetry will not scatter light, any defects, be it roughness, subsurface defects, grain structure, or particulate contamination, will scatter light into directions away from the specular or transmitted directions. It is therefore common to measure the bidirectional reflectance distribution function (BRDF), the fraction of incident light scattered per unit projected solid angle, or a solid-angle-integrated BRDF, to automate the assessment of the condition of materials such as bare silicon wafers, magnetic and optical storage media, mirrors, flat panel displays or other high quality optical materials.[2,3] Although different characteristic defects on any particular material sometimes have signature BRDFs that allow them to be distinguished, the BRDF lacks the general capability of unambiguously distinguishing between different sources of scatter.

On the other hand, the polarization of the light can indicate the path that the light followed during its trajectory. For example, light scattered by a particle above the surface of a material undergoes different trajectories than light which is scattered by roughness of a surface or by a defect below a surface. This effect is expected to be most pronounced for scattering of obliquely incident light into directions out of the plane of incidence, since these directions allow the viewing instrument to best observe the rotations of the electric field that occur upon refraction and reflection. Therefore, the polarization of out-of-plane scattered light should strongly indicate the sources of that scattered light.

Although polarized light scattering has been prevalent in studies of scattering in particles,[4,5] its use has been limited in the study of surfaces.[6-10] Much of this disuse has been a combined result of instrumentation issues and the interpretation of the results.

2

From the instrumentation side, measurements of light scattered out of the plane of incidence add extra degrees of freedom that are not present in the measurements of free particle scattering. On the interpretation side, few models have guided the experimentalist to the quickest and most efficient measurement. For example, the elements of the Mueller matrix BRDF, the polarimetric generalization of the BRDF, do not necessarily map directly onto those properties of the material which are relevant to understanding the origin of the scattered light. For example, one cannot simply take a particular element of the Mueller matrix BRDF and assign its magnitude to the density of a particular type of defect.

It is shown in this paper that a less generalized polarimetric treatment of the scattered light, bidirectional ellipsometry,[11] enables one to determine the location of scattering centers. In bidirectional ellipsometry, light with a particular linear polarization state is incident onto the surface, and the direction of the polarization of the scattered light is mapped out with a detection polarizer, yielding a principal angle of polarization, η, and a degree of linear polarization, P_{L}. It is shown that the value of η can be a sensitive measure of the origin of the scattered light.

In Section 2, simple model predictions for scattering from subsurface spheres, microroughness, and facets will be reviewed. The experiment by which these models will be tested will be outlined in Sec. 3. The results of these measurements will be presented in Sec. 4. Section 5 will discuss these results, comparing them to the model predictions. Finally, the conclusions of the paper will be set forth in Sec. 6.

2. THEORY

The coordinate system used to describe the incident and scattered light directions and polarizations is outlined in Fig. 1. The z axis coincides with the surface normal, and

light is assumed to be incident at an angle θ_i in the x-z plane. The direction of scattered light is parameterized by its polar angle θ_r and azimuthal angle ϕ_r. The basis set used to describe the polarization will be $\{\hat{\mathbf{s}}, \hat{\mathbf{p}}, \hat{\mathbf{k}}\}$, where $\hat{\mathbf{k}}$ is a unit vector in the direction of propagation, $\hat{\mathbf{s}}$ is a unit vector perpendicular to the plane of incidence (or viewing), and $\hat{\mathbf{p}} = \hat{\mathbf{k}} \times \hat{\mathbf{s}}$ is a unit vector in the plane of incidence (or viewing). There is a separate basis set for the incident and the scattered light, denoted by the subscripts i and r, respectively. The substrate material is assumed to have a complex dielectric constant ϵ at the wavelength of the incident light, λ.

Theories for scattering from particulate contaminants and subsurface defects in the Rayleigh limit, from microtopography, and from facets have been developed elsewhere.[12,13] In this section, we summarize the results of the subsurface defect and microroughness theories. Each of these theories predicts the form of the Jones scattering matrix,

$$\begin{pmatrix} E_s^{\text{scat}} \\ E_p^{\text{scat}} \end{pmatrix} = \frac{A \exp(ikR)}{R} \begin{pmatrix} q_{ss} & q_{ps} \\ q_{sp} & q_{pp} \end{pmatrix} \begin{pmatrix} E_s^{\text{inc}} \\ E_p^{\text{inc}} \end{pmatrix},$$

($k = 2\pi/\lambda$) which relates the components of the scattered electric field, $\mathbf{E}^{\text{scat}}$, at a distance R from the sample, to those of the incident electric field, $\mathbf{E}^{\text{inc}}$. An overall factor, A, which is common to all four elements of the matrix, does not affect the polarization of the light and will not be discussed in this paper. For comparison with experimental results, the scattering Jones matrix can be converted to its Mueller representation using a standard relationship found in the literature.[4,5]

Spheres small enough to be considered in the Rayleigh limit located below a surface will lead to a Jones scattering matrix, with elements given by[12]

$$q_{ss}^{\text{sub}} = k \cos \phi_r / [(k_{zi} + k_{zi}')(k_{zr} + k_{zr}')], \tag{1a}$$

$$q_{ps}^{\text{sub}} = -k_{zi}' \sin \phi_r / [(\epsilon k_{zi} + k_{zi}')(k_{zr} + k_{zr}')], \tag{1b}$$

$$q_{sp}^{\text{sub}} = -k_{zr}' \sin \phi_r / [(k_{zi} + k_{zi}')(\epsilon k_{zr} + k_{zr}')], \qquad (1c)$$

and

$$q_{pp}^{\text{sub}} = (k_{xyi}k_{xyr} - k_{zi}'k_{zr}' \cos \phi_r)/[(\epsilon k_{zi} + k_{zi}')(\epsilon k_{zr} + k_{zr}')], \qquad (1d)$$

where

$$k_{zj} = k \cos \theta_j,$$

$$k_{xyj} = k \sin \theta_j,$$

$$k_{zj}' = k\sqrt{\epsilon - \sin^2 \theta_j},$$

where j is either i or r. This model accounts for refraction at the interface and transmission of light into and out of the material. The correlations between defects, the penetration of the light into the material, the escape of the scattered light out of the material, the characteristic optical constant and size of the defect, and the wavelength of the light, λ, do not effect the polarization, but rather contribute to terms common to all four Jones matrix elements.

In the smooth surface limit, where first-order vector perturbation theory (Rayleigh-Rice theory) can be applied, the scattering from microroughness has a characteristic Jones matrix with elements given by[14−16]

$$q_{ss}^{\text{rough}} = k \cos \phi_r / [(k_{zi} + k_{zi}')(k_{zr} + k_{zr}')], \qquad (2a)$$

$$q_{ps}^{\text{rough}} = -k_{zi}' \sin \phi_r / [(\epsilon k_{zi} + k_{zi}')(k_{zr} + k_{zr}')], \qquad (2b)$$

$$q_{sp}^{\text{rough}} = -k_{zr}' \sin \phi_r / [(k_{zi} + k_{zi}')(\epsilon k_{zr} + k_{zr}')], \qquad (2c)$$

and

$$q_{pp}^{\text{rough}} = (\epsilon k_{xyi}k_{xyr} - k_{zi}'k_{zr}' \cos \phi_r)/[(\epsilon k_{zi} + k_{zi}')(\epsilon k_{zr} + k_{zr}')]. \qquad (2d)$$

Again, the surface height correlation function, or the power spectrum of the surface height function, and the optical wavelength contribute only to terms common to all four

5

elements, and therefore do not effect the polarization. Although the results of the micro-roughness model can be rigorously derived by expanding the boundary conditions to first order in the surface height function, the results are equivalent to radiation from dipoles below the surface created by the electric field above the surface (or vice versa).[17] This result differs from that of the defect model, which assumes a dipole moment is generated by the field at the location of the defect (below the surface), radiating from that same location.

It can be seen from Eqs. (1) and (2) that the q_{ss}, q_{ps}, and q_{sp} Jones matrix elements for the two mechanisms are identical, and that the q_{pp} elements differ, and then only if the θ_i and θ_r are nonzero. To exploit the polarization of scattered light to distinguish between these two mechanisms, it is necessary that some p-polarized light be involved in both the incident and scattered light, that there be some contribution from at least one of the q_{ss}, q_{ps}, and q_{sp} Jones matrix elements, that the light be incident at an oblique angle, and that the viewing angle be oblique. Comparison of the q_{pp} elements suggests that further contrast between the two mechanisms can be achieved if ϕ_r is varied; that is, one views the sample out of the plane of incidence. This contrast is then maximized by using either purely p-polarized incident light or p-polarized viewing light.

The conditions outlined above, allowing a distinction between the two mechanisms by bidirectional ellipsometry, are also met for in-plane measurements with light incident with a combination of s- and p-polarizations, e.g. 45° polarized light. However, this practice relies on interference between the q_{pp} element and the three other elements, whereas the practice of measuring the polarization of out-of-plane scattered light for p-polarized incident light (or visa versa) relies only on interference between the q_{pp} element and one other element. For this reason, it is expected that the polarization of out-of-plane scattered light for p-polarized incident light will be more sensitive to the scattering mechanism.

When the roughness is much larger than the wavelength of the light, then a specular point, or facet, approximation is expected to be valid.[13] This model assumes that light is scattered by specular reflection by facets on the surface, the distribution being determined by the distribution of surface slopes, and the polarization being determined by reflection in the local reference frame for each facet. For brevity, the scattering matrix will not be reproduced here, but the results will be used in a comparison to the data for the rough etched backside of a silicon wafer. Like the microroughness and subsurface defect models, light scattered in the specular point approximation is completely polarized.

3. EXPERIMENT

The Goniometric Optical Scatter Instrument (GOSI), which was used to perform the measurements described in this paper, is described elsewhere.[18,19] Briefly, the second harmonic of a cw Nd:YAG laser ($\lambda = 532$ nm) is incident onto a sample at an angle θ_i, and light scattered into the direction defined by the angles $\{\theta_r, \phi_r\}$ is collected (see Fig. 1). The polarization state of the incident light is selected with a fixed linear polarizer followed by a rotatable $\lambda/2$ linear retarder. The polarization state of the scattered light is analyzed with a rotatable $\lambda/2$ linear retarder followed by a fixed linear polarizer. Although a bidirectional ellipsometric measurement can be carried out by fixing the incident light polarization while rotating the detection polarization optics, all of the measurements described in this paper were made by measuring the 3×3 non-handed Mueller matrix using a $(\omega, 4\omega)$ scheme,[20] whereby the receiving retarder is rotated at four times the rate of the incident light retarder. The signal is measured at 16 evenly spaced intervals, and the 9 elements of the 3×3 non-handed Mueller matrix $[M_{ij}, (i,j = 0,1,2)]$ are determined from the Fourier transform of those signals. Since only linear polarized light is used in these measurements, the fourth row and column of the Mueller matrix are never determined.

When p-polarized light is incident upon the sample, the first three elements of the Stokes vector of the scattered light are given by $S_0 = M_{00} - M_{01}$, $S_1 = M_{10} - M_{11}$, and $S_2 = M_{20} - M_{21}$. The angle $\eta^{(\mathrm{p})}$ that the principal axis of the polarization ellipse makes with respect to the $\hat{\mathbf{s}}$ axis when the incident light is p-polarized can then be determined from the Stokes vector elements S_i to be[21]

$$\eta^{(\mathrm{p})} = \frac{1}{2}\arctan(S_1, S_2), \tag{3}$$

where $\arctan(x, y)$ is the argument of $x + iy$. As a measure of the degree to which the light is linearly polarized, the degree of linear polarization when p-polarized light is incident on the sample is

$$\begin{aligned}
P_{\mathrm{L}}^{(\mathrm{p})} &= (f_{\max} - f_{\min})/(f_{\max} + f_{\min}) \\
&= [(S_1)^2 + (S_2)^2]^{1/2}/S_0,
\end{aligned} \tag{4}$$

where $f_{\max}$ and $f_{\min}$ are the maximum and minimum scattered light signals as an analyzing linear polarizer is rotated, respectively (see Fig. 2). For linearly polarized light, $P_{\mathrm{L}}^{(\mathrm{p})} = 1$, and for purely depolarized light or circularly polarized light, $P_{\mathrm{L}}^{(\mathrm{p})} = 0$.

By concentrating attention on the principal axis of the polarization ellipse, certain issues can often be ignored. Foremost of these is the scattering from other objects in the room which are illuminated by the specular beam. This light is most likely to be highly depolarized, and therefore will have little effect on the measurement of $\eta^{(\mathrm{p})}$.

For all of the measurements reported in this paper, the incident angle was $\theta_{\mathrm{i}} = 45°$ and the polar scattering angle was $\theta_{\mathrm{r}} = 45°$. The azimuthal scattering angle ϕ_{r} was varied so that the polarization of scattered light through a cone in the scattering hemisphere was mapped out, and all but the extremes of the domain correspond to scattering out of the plane of incidence. From the Bragg relationship, there exists a direct mapping

of angles (θ_i, θ_r, ϕ_r) to the spatial frequency (inverse periodicity) of the roughness being probed. When $\theta_i = \theta_r$, the spatial frequency is $f = 2\sin(\theta_i)\sin(\phi_r/2)/\lambda$.

The polarization of optical scattering from a variety of samples was measured. Each sample was chosen for its capability of demonstrating the theories above. Four silicon samples ($\epsilon = 16.40 + 0.12i$ at $\lambda = 532$ nm from Ref. (22)) were measured: two (Si1 and Si2) which were photolithographically designed to exhibit surface microroughness of two different levels;[23] a third (Si3) which was the rough etched backside of a silicon wafer; and a fourth (Si4) which was a polished Czochralski-grown silicon wafer that exhibited a significant degree of haziness from an unknown source. As an indication of the relative scattering levels of these four samples, the BRDF levels in the $\theta_i = 0°$ and $\theta_r = 45°$ configuration were approximately 10^{-6} sr^{-1}, 10^{-4} sr^{-1}, 10^{-2} sr^{-1}, and 10^{-6} sr^{-1}, respectively.

To further test the validity of the microroughness model with a metallic sample, a 110 nm thick film of titanium nitride grown on a silicon wafer was considered (TiN). Atomic force and scanning electron microscopies have typically found these surfaces to have a high degree of roughness. This film exhibited a $0°/45°$ BRDF of approximately 10^{-4} sr^{-1}. The thickness of the film is sufficiently great that the film can be treated as a bulk titanium nitride sample. The dielectric constant of titanium nitride at 532 nm is reported by Ref. (24) to be $\epsilon = -2.3 + 4.8i$. However, a rotating analyzer specular ellipsometry measurement, performed at an incident angle of 55°and fitted to the results of a two-phase model, yielded a value of $\epsilon = 1.3 + 5.6i$. The bidirectional ellipsometry results presented in this paper were better fit with the somewhat different value of $\epsilon = 1.6 + 4.6i$.

Two additional samples were used to test the subsurface defect model. The first (FS) was a highly polished piece of high grade fused silica. Due to its polycrystaline

9

structure, fused silica exhibits a small degree of bulk Rayleigh scatter. The scattering extinction coefficient was measured to be about 2×10^{-5} cm^{-1} (base e) at 532 nm. At angles close to the specular direction the scattered light is expected to be dominated by surface figure, while at larger angles, the total scatter is dominated by the scatter from the bulk. The second of these samples (ZD) was a polished piece of glass ceramic (Zerodur[25]), a material whose scattering extinction coefficient was measured to be about 7×10^{-2} cm^{-1} (base e).

A useful feature of bidirectional ellipsometry is its ability to distinguish between different scattering mechanisms. A series of Schott[25] UG1 visible light absorbing glass samples[26] was chosen, each ground and polished to different degrees so as to exhibit a variety of BRDF levels, and are expected to exhibit a combination of microroughness and subsurface damage. These samples (BgA, BgB, BgC, BgD, BgE, and BgF), which were prototypes developed as BRDF calibration standards,[26] exhibited BRDF levels in the $0°/45°$ incident/viewing configurations of approximately 7×10^{-6} sr^{-1}, 3×10^{-5} sr^{-1}, 2×10^{-3} sr^{-1}, 7×10^{-3} sr^{-1}, 9×10^{-3} sr^{-1}, and 1×10^{-2} sr^{-1}, respectively. The dielectric constant for all of the glass samples was assumed to be approximately $\epsilon = 2.25$.

The random and systematic measurement uncertainties for η and P_L can be estimated by performing a series of measurements of these values with the receiver in the path of the incident light and without the sample present. A series of eighty measurements yielded values of $\eta = 90.08°$ and $P_L = 0.9993$. These values differ from the theoretical values of $\eta = 90°$ and $P_L = 1$ due to systematic errors. The standard deviations, $\sigma_\eta = 0.01°$ and $\sigma_{P_L} = 0.0003$, represent the respective random uncertainties for a single measurement. The random uncertainties associated with the measurements are significantly larger and are similar to the apparent fluctuations about their trends. Other systematic errors may contribute to uncertainties with the sample present. Although

10

a complete discussion of these uncertainties is beyond the scope of this paper, the expanded uncertainties[27] of η and P_L are not expected to exceed 5°and 0.05, respectively.

4. RESULTS AND DISCUSSION

Figures 3–6 show the results of bidirectional ellipsometric measurements on all of the samples, grouped by material. For each sample set, we show the principal angle of the polarization, $\eta^{(p)}$, and the degree of linear polarization, $P_L^{(p)}$. The predictions of the subsurface defect and microroughness theories, using Eqs. (1) and (2), respectively, are shown with each set of data. Since Fig. 3 also contains data for the rough etched backside of a silicon wafer, the predictions of the facet model are also included. All three theories predict $P_L^{(p)} \sim 1$, except when applied to the metallic TiN sample.

The three rough silicon samples, Si1, Si2, and Si3, shown in Fig. 3, appear to follow the microroughness model very well. (Sample Si4 will be discussed later in this section.) The angle $\eta^{(p)}$ lies close to the model, and the degree of linear polarization, P_L, remains high. Deviations from $P_L = 1$ are most evident for sample Si1, for which the sample scatter is very low and extraneous signals not associated with the sample, such as Rayleigh scatter in the air surrounding the sample or scatter in the room from the specularly reflected beam, are most likely to dominate. For scattering angles ϕ_r less than 40°, the degrees of linear polarization are all 95% or higher.

It is somewhat surprising the degree to which sample Si3 follows the microroughness model. The Si3 sample is not specular, so that the smooth surface limit would not be expected to apply. Close inspection of the $\eta^{(p)}$ data in Fig. 3 suggests that, while the Si1 and Si2 samples are randomly scattered about the theoretically predicted curve, a systematic deviation between the microroughness theory and the $\eta^{(p)}$ data for sample Si3 exists. For that reason, the prediction of the specular point model has been included

with the data in Fig. 3. It can be seen that the data for sample Si3 follows consistently between the microroughness model and the specular point model, perhaps even following the specular point model for $\phi_r < 40°$. This result suggests that the light scattered by a very rough surface, in some situations, may be considered as a combination of light scattered in the two limiting approximations. In a regime where multiple scattering in the specular point approximation occurs, further refinement of the theory, however, would be expected, and would yield true depolarization of the light.

The light scattered by microroughness for p-polarized incident light is expected to be linearly polarized. Although at large scattering angles, $P_L^{(p)}$ deviates from unity, the excellent agreement between theory and experiment for $\eta^{(p)}$ suggests that the increasing depolarization is occurring because of the growing relative contribution of minority scattering mechanisms. For example, microrough surfaces might be expected to yield a small degree of subsurface features. Furthermore, nearly all surfaces include some oxide layer, which may modify the scattering characteristics to some degree.[28] As mentioned above, for the low scatter silicon samples (Si1, Si2, and Si4), some of the apparent depolarization may be due to background scatter resulting from the specular beam striking the diffusely reflecting walls of the room or electrical cables on the goniometer. For Sample Si1, Rayleigh scatter in the air surrounding the sample may also be contributing to a background.[29] For sample Si3, which is very rough, the degree of polarization is greater than 0.90, suggesting that large amounts of roughness do not necessarily cause large amounts of depolarization.

Figure 4 shows the results for the TiN sample. Unlike the samples shown in Fig. 3, the metallic nature of TiN causes some degree of elliptical polarization, indicated by the model predictions for $P_L^{(p)}$ deviating from unity. The solid curves in Fig. 4 represent the predictions of the model using a dielectric constant $\epsilon = 1.6 + 4.6i$, which appears to fit

both the $\eta^{(\mathrm{p})}$ and $P_{\mathrm{L}}^{(\mathrm{p})}$ very well. Deviations between the theory and the measurement for $P_{\mathrm{L}}^{(\mathrm{p})}$ are typically within 0.01, while those for $\eta^{(\mathrm{p})}$ are within $0.6°$.

The excellent agreement between the theory and experiment for microroughness, shown for rough silicon in Fig. 3 and for TiN in Fig. 4, implies that the polarization of light scattered by microroughness is not determined by the exact details of the surface height profile, but is a unique signature of the scattering mechanism. It therefore suggests that scatterometers can be designed to be blind to microroughness. For example, a device may be constructed with a number of detectors, each viewing a particular scattering direction, and each with a polarizer aligned to null the signal from microroughness.[30] Such a device would collect light over a large solid angle, be microroughness-blind, and therefore be more sensitive to other sources of scatter, such as subsurface defects and particulate contamination.

The $\eta^{(\mathrm{p})}$ data for the glass ceramic sample (ZD), shown in Fig. 5, follows the subsurface defect model very well. The rather low $P_{\mathrm{L}}^{(\mathrm{p})}$ in sample ZD is expected. The scattering extinction coefficient is very high so that multiple scattering will occur, the size of the grains is probably not small enough for Rayleigh scattering to be applicable, and those grains are not all of the same size and shape. The ability for bidirectional ellipsometry to extract a primary direction of polarization in such good agreement with the theory may at first glance be surprising, since the models for scattering from subsurface defects assume the scatterers can be treated in the Rayleigh approximation. That is, the scattering centers are assumed to be point sources which polarize in the direction of the local electric field and locally radiate an electric field proportional to $\mathbf{k} \times \mathbf{k} \times \mathbf{p}$, where $\mathbf{k}$ is the wavevector of the scattered light, and $\mathbf{p}$ is the induced dipole moment. However, simple symmetry arguments can be invoked to show that a random distribution of scattering centers will also polarize and radiate, on average, in the same manner. Therefore, when the scatterers are randomly oriented in the material, the primary direction of the

13

polarization, $\eta^{(p)}$, is an indication of the local environment of the scatterers. Certainly, if all the defects within the illuminated region are aligned in a certain manner, and are not random, then there will be a preferential direction differing from that predicted by the Rayleigh approximation. Similarly, if a single non-Rayleigh scattering center is in the illuminated region, then the polarimetric behavior will reflect details of that scattering center, rather than that of an ensemble average.

The $\eta^{(p)}$ data for fused silica, also shown in Fig. 5, agree very well with the subsurface model for out-of-plane scattering angles ϕ_r greater than $\sim 75°$. At these angles the scattered light within the field of view of the receiver is consistent with the hypothesis that it is dominated by the Rayleigh scattering in the material, which is predominantly isotropic. For ϕ_r closer to the specular, however, the polarization of the scattered light deviates from the subsurface model and approaches the microroughness model. At these angles the scattered light is likely to be dominated by the surface finish of the sample. This behavior is not observed for sample ZD, presumably since the subsurface scatter is over three orders of magnitude greater than that for sample FS. The fact that these two scattering sources can be distinguished in fused silica suggests that surface finish can be measured by polarized scattered light techniques, despite the existence of subsurface scatter.

Although the black glass data for $\eta^{(p)}$, shown in Fig. 6, appear to follow the microroughness model, they show a marked deviation toward the subsurface defect model, suggesting that both mechanisms are contributing to the scattered light, with a greater contribution arising from microroughness over most of the range of angles. This behavior is not surprising since some subsurface damage inevitably occurs during the polishing process. The ability for bidirectional ellipsometry to distinguish between the two mechanisms, and possibly to assign a magnitude to the two contributions, suggests that the

14

technique could prove useful in diagnosing manufacturing processes, where the types of defects that are created may be indicative of particular process deviations.

The data for sample Si4, included in Fig. 3, shows a marked deviation from that of the other silicon samples. This sample, which was purchased as a prime silicon wafer exhibited a significant degree of optical scatter. Analysis of the angle $\eta^{(p)}$ suggests, however, that the scatter is not originating from surface roughness, but rather from some sort of subsurface defects. "Crystal originated particles," as the semiconductor industry refers to them, are common under certain wafer growth conditions, and consist of small oxide and vacancy precipitates in the material.[31] The fact that these localized defects scatter light has earned them their misnomer. The results of this paper, however, suggest that the polarization of the scattered light can be used to distinguish scatter resulting from microroughness from that resulting from subsurface defects.

Models exist for scattering from particles on surfaces which predict the polarization of the scattered light to be different than that predicted for subsurface defects or microroughness. For example, for very small particles on the silicon or TiN samples, the light scattered by p-polarized incident light is expected to have $\eta^{(p)} = 90°$ for all ϕ_r in the $\theta_i = \theta_r = 45°$ geometry.[12] Although experimental results for bidirectional ellipsometry measurements of particles on surfaces will be presented elsewhere, the technique of bidirectional ellipsometry should prove useful for distinguishing such particles from other sources of scatter such as microroughness. It is reasonable to speculate that bidirectional ellipsometry will be as applicable to the study of defects in thin films and roughness at thin film interfaces as specular ellipsometry is at characterizing thin films. The location of the source of scattering in a layered system, whether it be roughness in one of the interfaces, or disorder in one of the layers, may be discernible with bidirectional ellipsometry.[32]

15

5. CONCLUSION

The results presented in this paper demonstrate that the principal polarization, $\eta^{(\mathrm{p})}$, of scattered light from a variety of sources agrees very well with some simple models for optical scattering. Scattering from surface microroughness and subsurface features have characteristic polarimetric signatures that allow these two mechanisms to be distinguished.

ACKNOWLEDGEMENTS

FIGURE CAPTIONS

Figure 1 The sample and beam coordinate systems.

Figure 2 A schematic of the intensity distribution measured by a rotating linear polarizer, defining the angle η and the maximum and minimum signals, $f_{\max}$ and $f_{\min}$, respectively. The axes are defined so that the viewer is looking into the scattered beam.

Figure 3 Results of bidirectional ellipsometry measurements for the four silicon samples (Si1, Si2, Si3, and Si4) as functions of the azimuthal scattering angle ϕ_r: (top) the degree of linear polarization ($P_{\mathrm{L}}^{(\mathrm{p})}$), and (bottom) the principal polarization angle $\eta^{(\mathrm{p})}$ for p-polarized incident light. The incident and scattering polar angles were both $45°$. The curves represent the models for surface microroughness (solid), subsurface defects (dashed), and facets (dotted).

Figure 4 Results of bidirectional ellipsometry measurements for the TiN sample as functions of the azimuthal scattering angle ϕ_r: (top) the degree of linear polarization ($P_{\mathrm{L}}^{(\mathrm{p})}$), and (bottom) the principal polarization angle $\eta^{(\mathrm{p})}$ for p-polarized incident light. The incident and scattering polar angles were both $45°$. The curves represent the models for surface microroughness (solid) and subsurface defects (dashed).

Figure 5 Results of bidirectional ellipsometry measurements for the two transparent samples (FS and ZD) as functions of the azimuthal scattering angle ϕ_r: (top) the degree of linear polarization ($P_{\mathrm{L}}^{(\mathrm{p})}$), and (bottom) the principal polarization angle $\eta^{(\mathrm{p})}$ for p-polarized incident light. The incident and scattering polar angles were both $45°$. The curves represent the models for surface microroughness (solid) and subsurface defects (dashed).

17

Figure 6 Results of bidirectional ellipsometry measurements for the six black glass samples (BgA, BgB, BgC, BgD, BgE, and BgF) as functions of the azimuthal scattering angle ϕ_r: (top) the degree of linear polarization ($P_L^{(p)}$), and (bottom) the principal polarization angle $\eta^{(p)}$ for p-polarized incident light. The incident and scattering polar angles were both $45°$. The curves represent the models for surface microroughness (solid) and subsurface defects (dashed).

REFERENCES

[1] J. C. Stover, *Optical Scattering: Measurement and Analysis*, (SPIE Optical Engineering Press, Bellingham, WA, 1995).

[2] J. C. Stover, ed., *Optical Scattering in the Optics, Semiconductor, and Computer Disk Industries*, Proc. SPIE 2541 (1995).

[3] J. C. Stover, ed., *Flatness, Roughness, and Discrete Defect Characterization for Computer Disks, Wafers, and Flat Panel Displays*, Proc. SPIE 2862 (1996).

[4] C. F. Bohren, and D. R. Huffman, *Absorption and Scattering of Light by Small Particles*, (Wiley, New York, 1983).

[5] H. C. v. d. Hulst, *Light Scattering by Small Particles*, (Dover, New York, 1981).

[6] R. E. Luna, "Scattering by one-dimensional random rough metallic surfaces in a conical configuration: several polarizations," Opt. Lett. **21**, 1418–1420 (1996).

[7] J. L. Pezzaniti, and R. A. Chipman, "Mueller matrix scatter polarimetry of a diamond-turned mirror," Opt. Eng. **34**, 1593–1598 (1995).

[8] E. L. Church, and J. C. Stover, "Surface haze in the Stokes-Mueller representation," in *Flatness, Roughness, and Discrete Defect Characterization for Computer Disks, Wafers, and Flat Panel Displays*, J. C. Stover, ed., Proc. SPIE **2862**, 54–68 (1996).

[9] E. R. Méndez, A. G. Navarrete, and R. E. Luna, "Statistics of the polarization properties of one-dimensional randomly rough surfaces," J. Opt. Soc. Am. A **12**, 2507–2516 (1995).

[10] S.-M. F. Nee, "Polarization of specular reflection and near-specular scattering by a rough surface," Appl. Opt. **35**, 3570–3582 (1996).

[11] T. A. Germer, C. C. Asmail, and B. W. Scheer, "Polarization of out-of-plane scattering from microrough silicon," Opt. Lett. **22**, 1284–1286 (1997).

[12] T. A. Germer, "Angular dependence and polarization of out-of-plane optical scattering from particulate contamination, subsurface defects, and surface microroughness," Appl. Opt. **36**, 8798–8805 (1997).

[13] D. E. Barrick, "Rough surface scattering based on the specular point theory," IEEE Trans. Ant. Prop. **AP-16**, 449–454 (1968).

[14] S. O. Rice, "Reflection of Electromagnetic Waves from Slightly Rough Surfaces," Comm. Pure and Appl. Math. **4**, 351–378 (1951).

[15] G. R. Valenzuela, "Depolarization of EM Waves by Slightly Rough Surfaces," IEEE Trans. Ant. Prop. **AP-15**, 552–557 (1967).

[16] D. E. Barrick, *Radar Cross Section Handbook*, (Plenum, New York, 1970).

[17] E. Kröger, and E. Kretschmann, "Scattering of light by slightly rough surfaces or thin films including plasma resonance emission," Z. Physik **237**, 1–15 (1970).

[18] C. C. Asmail, C. L. Cromer, J. E. Proctor, and J. J. Hsia, "Instrumentation at the National Institute of Standards and Technology for bidirectional reflectance distribution function (BRDF) measurements," in *Stray Radiation in Optical Systems III*, R. P. Breault, ed., Proc. SPIE **2260**, 52–61 (1994).

[19] T. A. Germer, and C. C. Asmail, "A goniometric optical scatter instrument for bidirectional reflectance distribution function measurements with out -of-plane and polarimetry capabilities," in *Scattering and Surface Roughness*, Z.-H. Gu, and A. A. Maradudin, ed., Proc. SPIE **3141**, 220–231 (1997).

[20] R. M. A. Azzam, "Photopolarimetric measurement of the Mueller matrix by Fourier analysis of a single detected signal," Opt. Lett. **2**, 148–150 (1978).

20

[21] R. A. Chipman, "Polarimetry," in *Handbook of Optics, Vol. II*, Michael Bass, ed., pp. 22.1–37 (McGraw-Hill, New York, 1995).

[22] E. D. Palik, *Handbook of Optical Constants of Solids*, (Academic, San Diego, 1985).

[23] B. W. Scheer, "Development of a physical haze and microroughness standard," in *Flatness, Roughness, and Discrete Defect Characterization for Computer Disks, Wafers, and Flat Panel Displays*, J. C. Stover, ed., Proc. SPIE **2862**, 78–95 (1996).

[24] E. D. Palik, *Handbook of Optical Constants of Solids II*, (Academic, San Diego, 1991).

[25] Certain commercial equipment, instruments, or materials are identified in this paper in order to specify the experimental procedure adequately. Such identification is not intended to imply recommendation or endorsement by the National Institute of Standards and Technology, nor is it intended to imply that the materials or equipment identified are necessarily the best available for the purpose.

[26] C. Asmail, J. Fuller, and R. Parks, "Status of Bidirectional Reflectance Distribution Function (BRDF) Calibration Standards Development," in *Quality and Reliability for Optical Systems*, J. W. Bilbro, and R. E. Parks, ed., Proc. SPIE **1993**, 44–53 (1993).

[27] B. N. Taylor, and C. E. Kuyatt, "Guidelines for Evaluating and Expressing the Uncertainty of NIST Measurement Results," Technical Note 1297 (NIST, Gaithersburg, 1994).

[28] J. M. Elson, "Light scattering from surfaces with a single dielectric overlayer," J. Opt. Soc. Am. **66**, 682–694 (1976).

[29] C. Asmail, J. Hsia, A. Parr, and J. Hoeft, "Rayleigh scattering limits for low-level bidirectional reflectance distribution function measurements," Appl. Opt. **33**, 6084-6091 (1994).

[30] T. A. Germer, and C. C. Asmail, "Microroughness-blind hemispherical optical scatter instrument," U.S. Patent Application filed (April 10, 1998).

[31] J. Ryuta, E. Morita, T. Tanaka, and Y. Shimanuki, "Crystal-originated singularities on Si wafer surface after SC1 cleaning," Jpn. J. Appl. Phys. **29**, L1947–L1949 (1990).

[32] T. A. Germer, "Application of bidirectional ellipsometry to the characterization of roughness and defects in dielectric layers," in *Flatness, Roughness, and Discrete Defect Characterization for Computer Disks, Wafers, and Flat Panel Displays II*, J. C. Stover, ed., Proc. SPIE **3275**, 121–131 (1998).
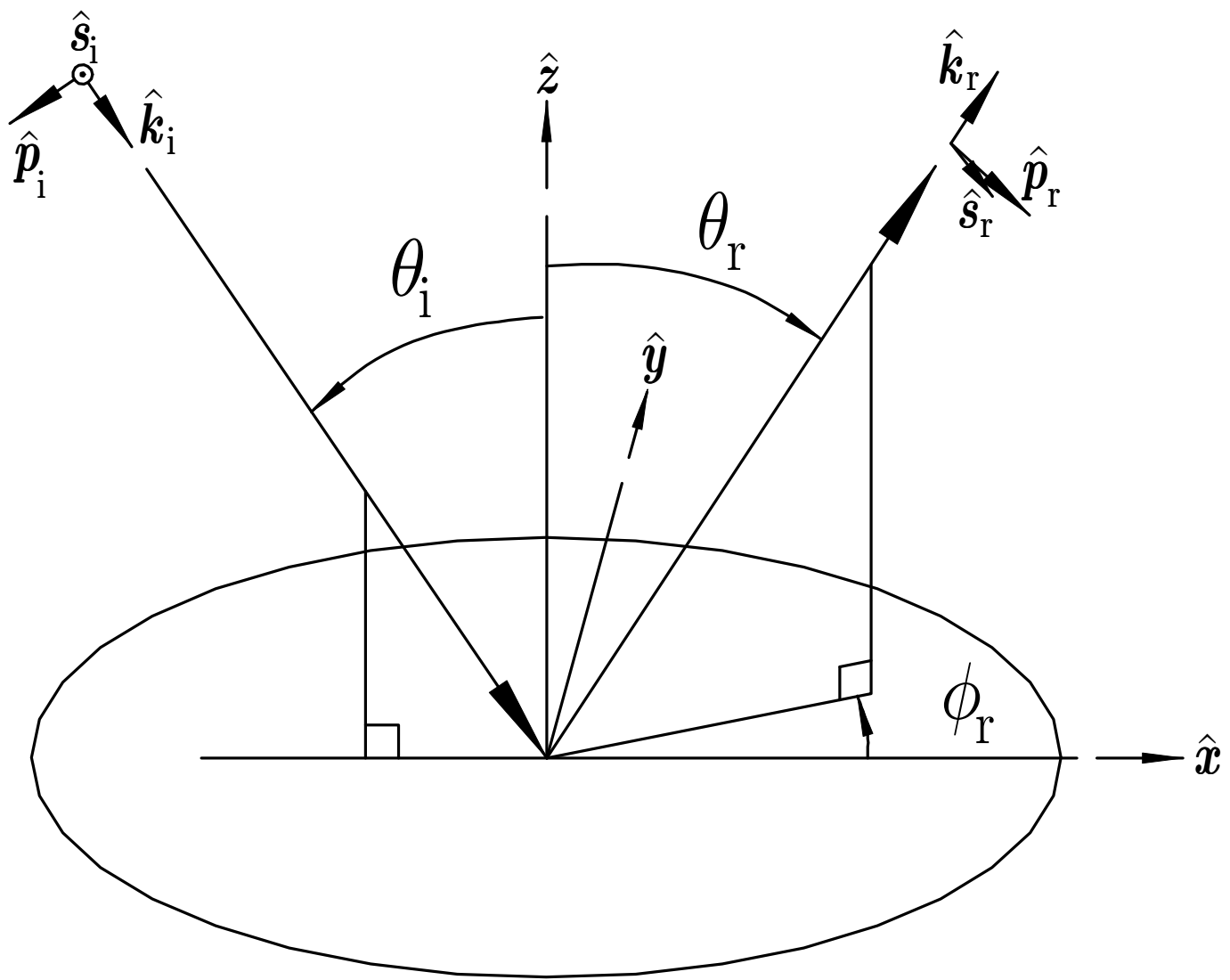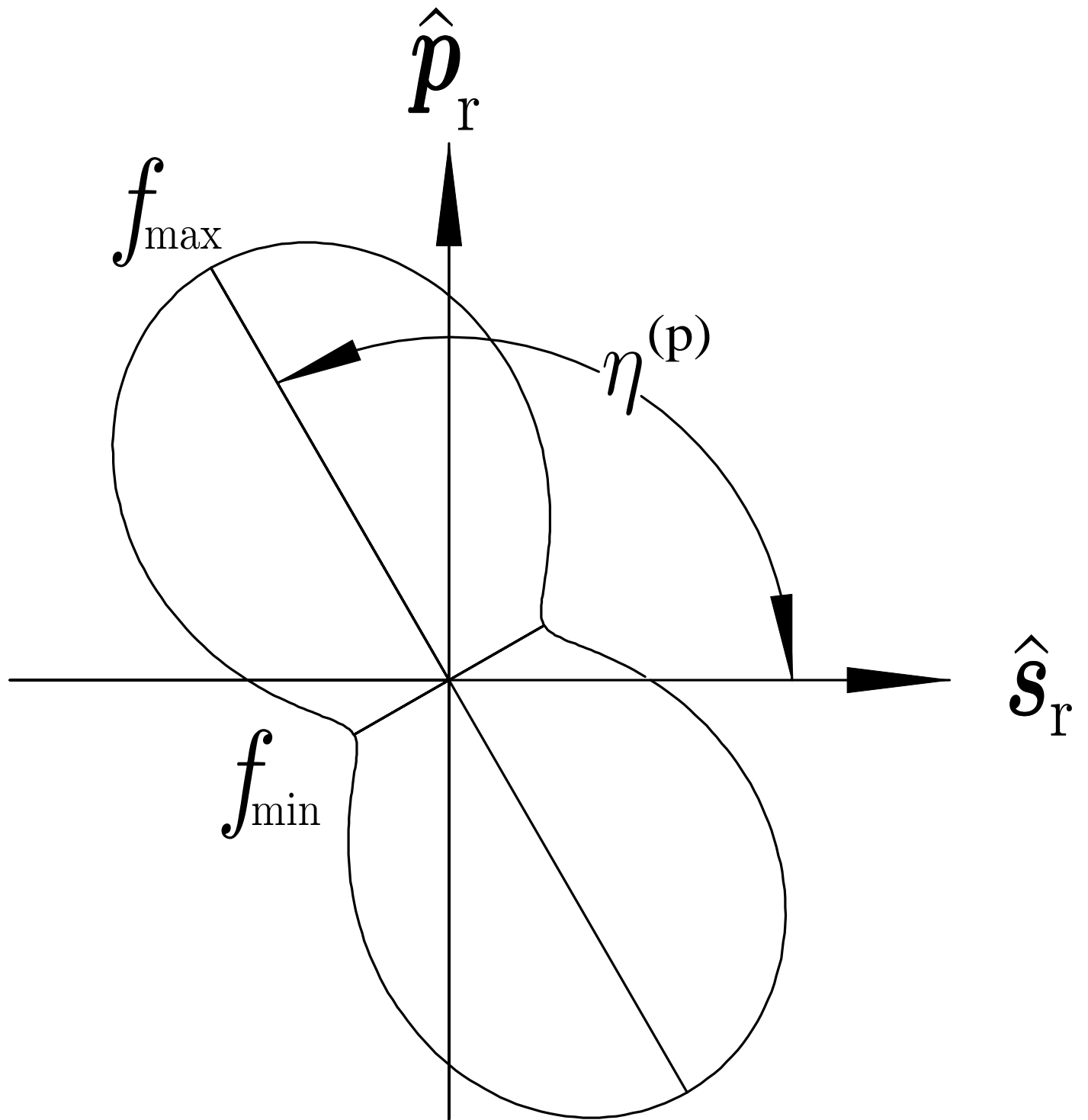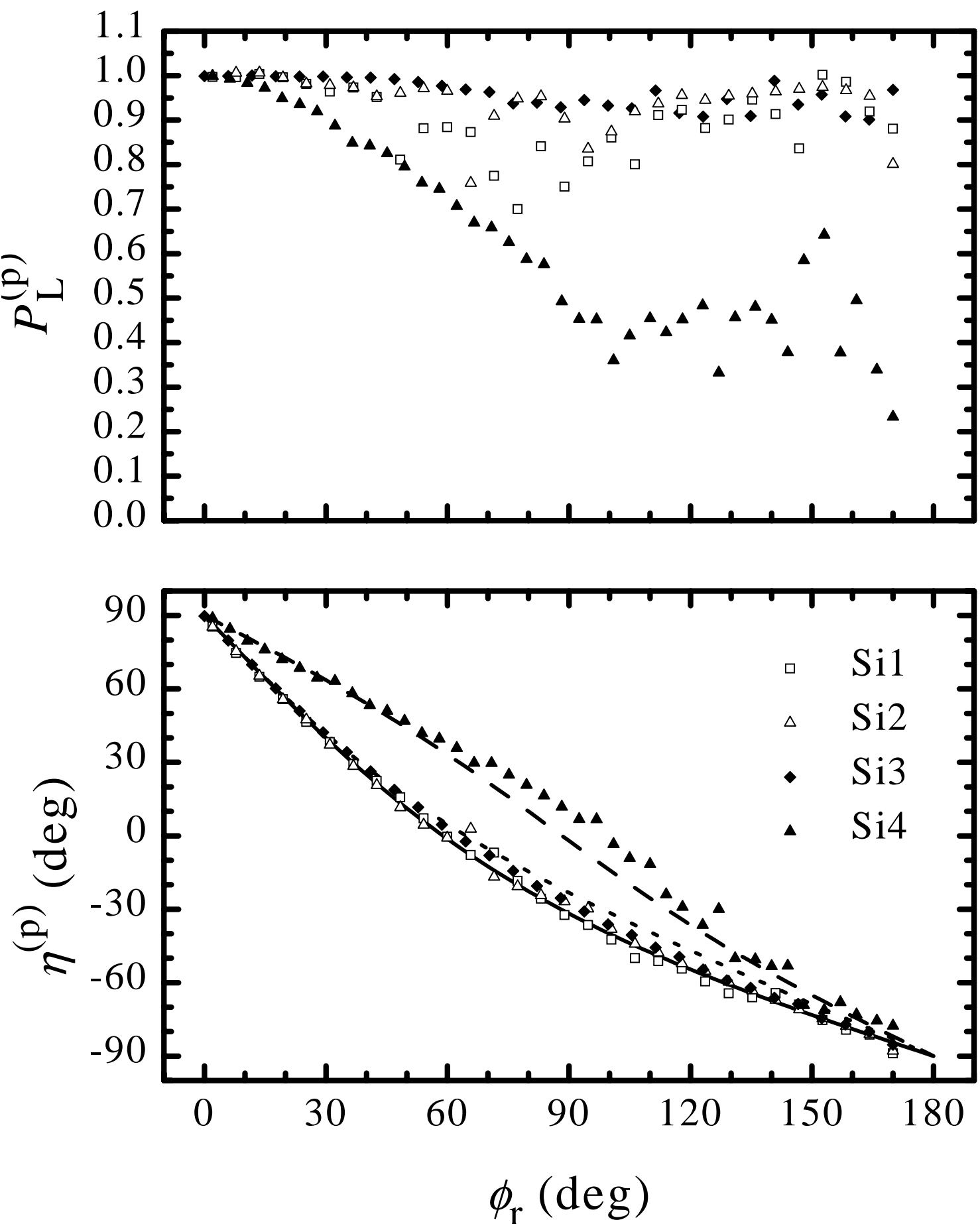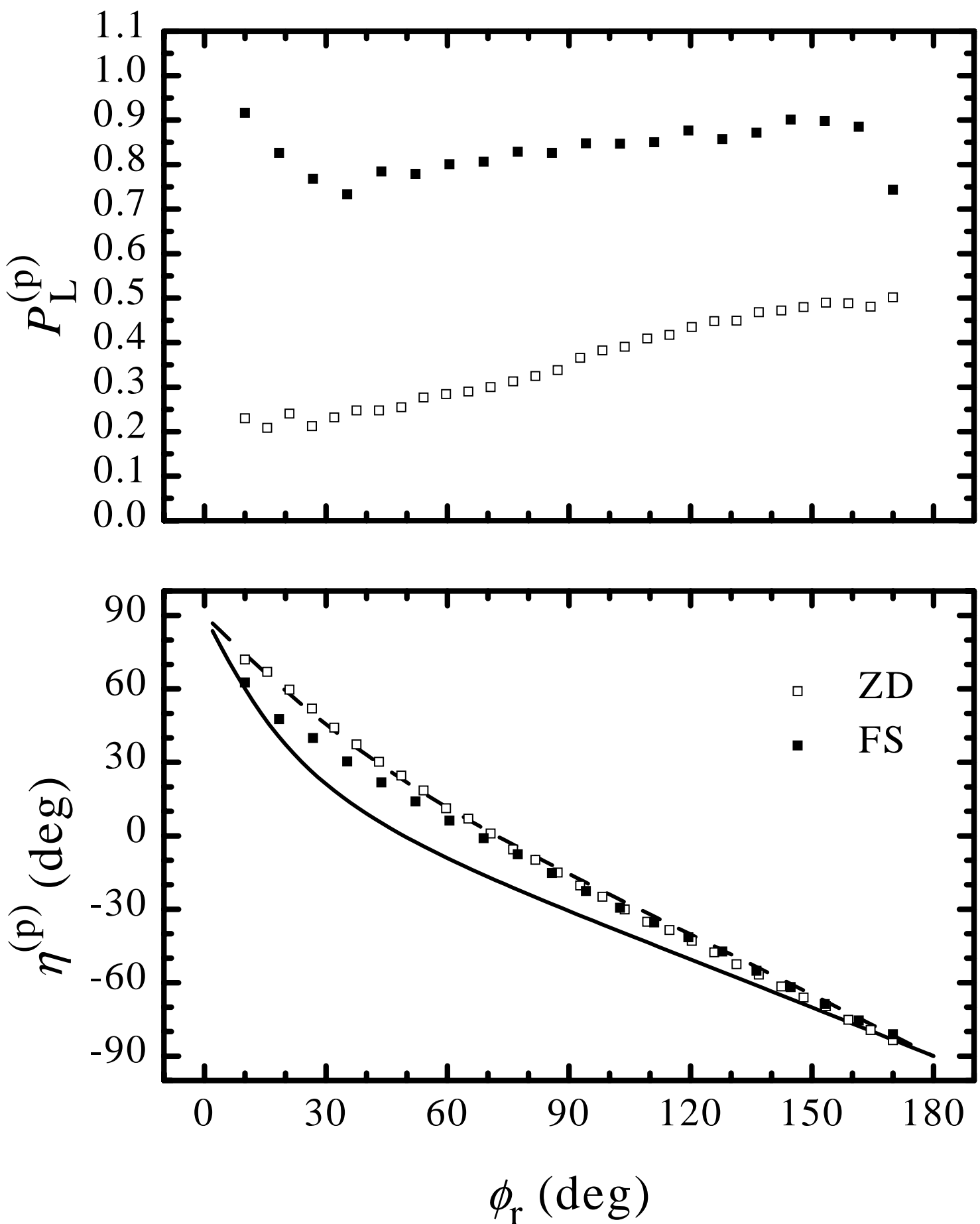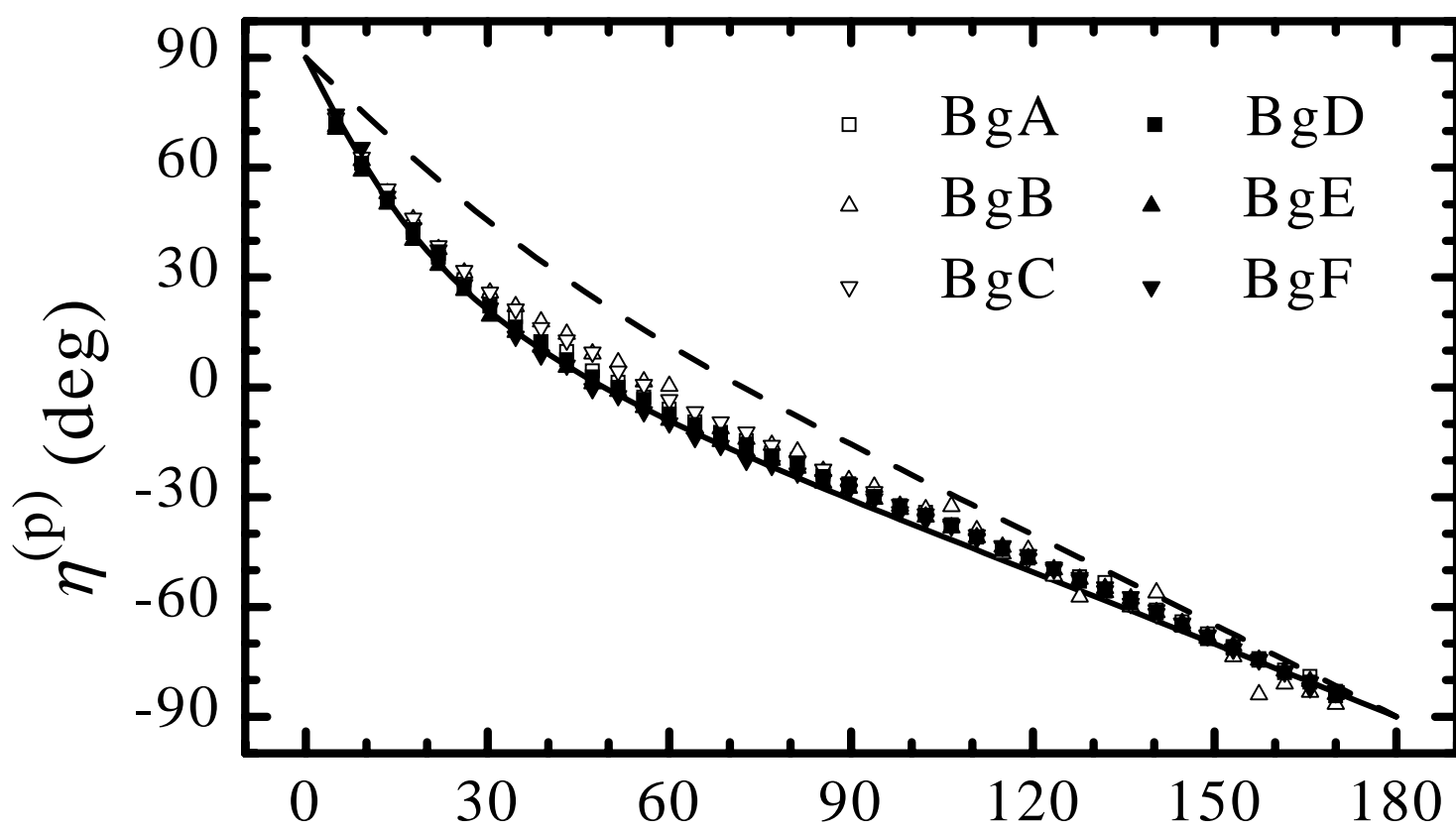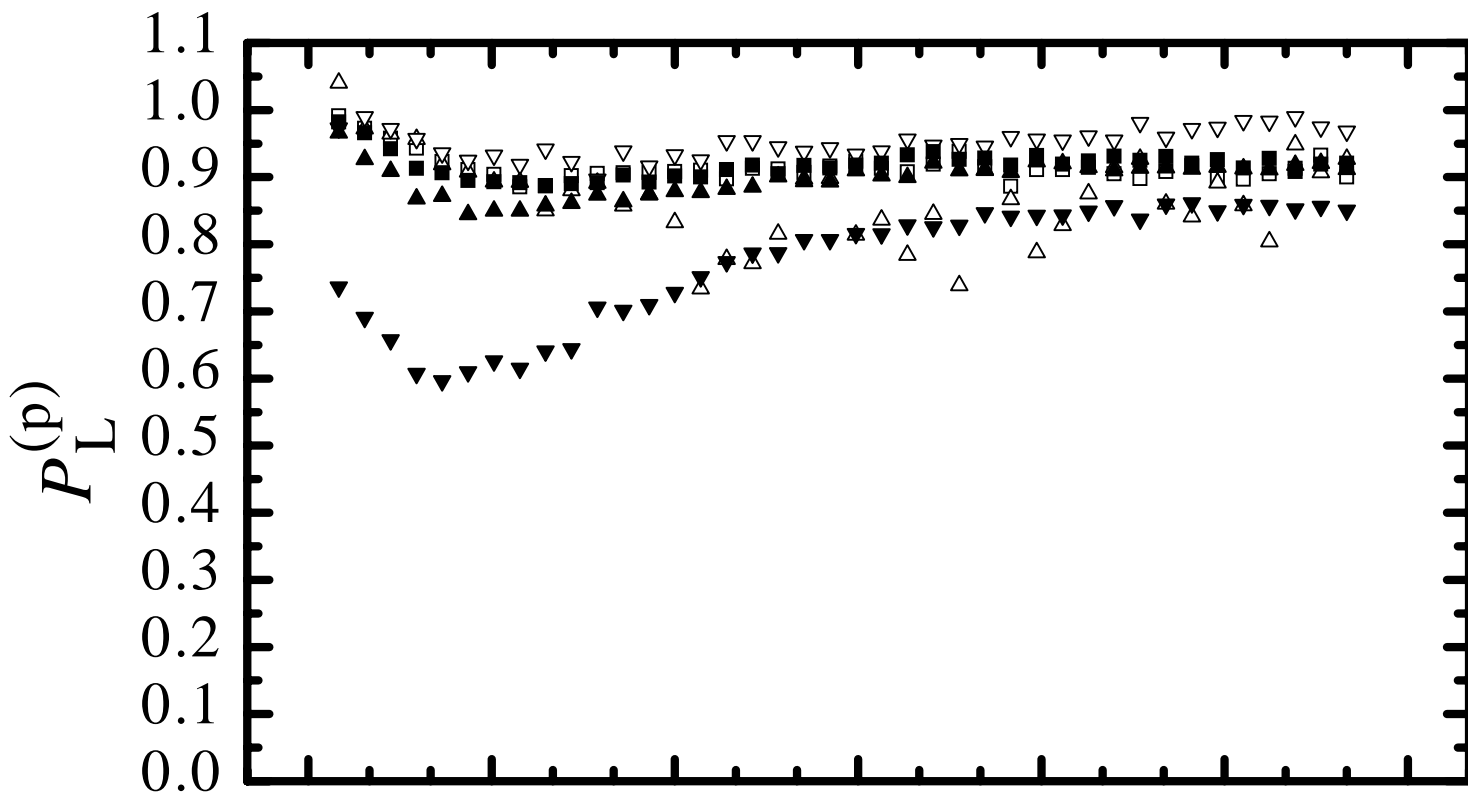
Germer and Asmail, Figure 3
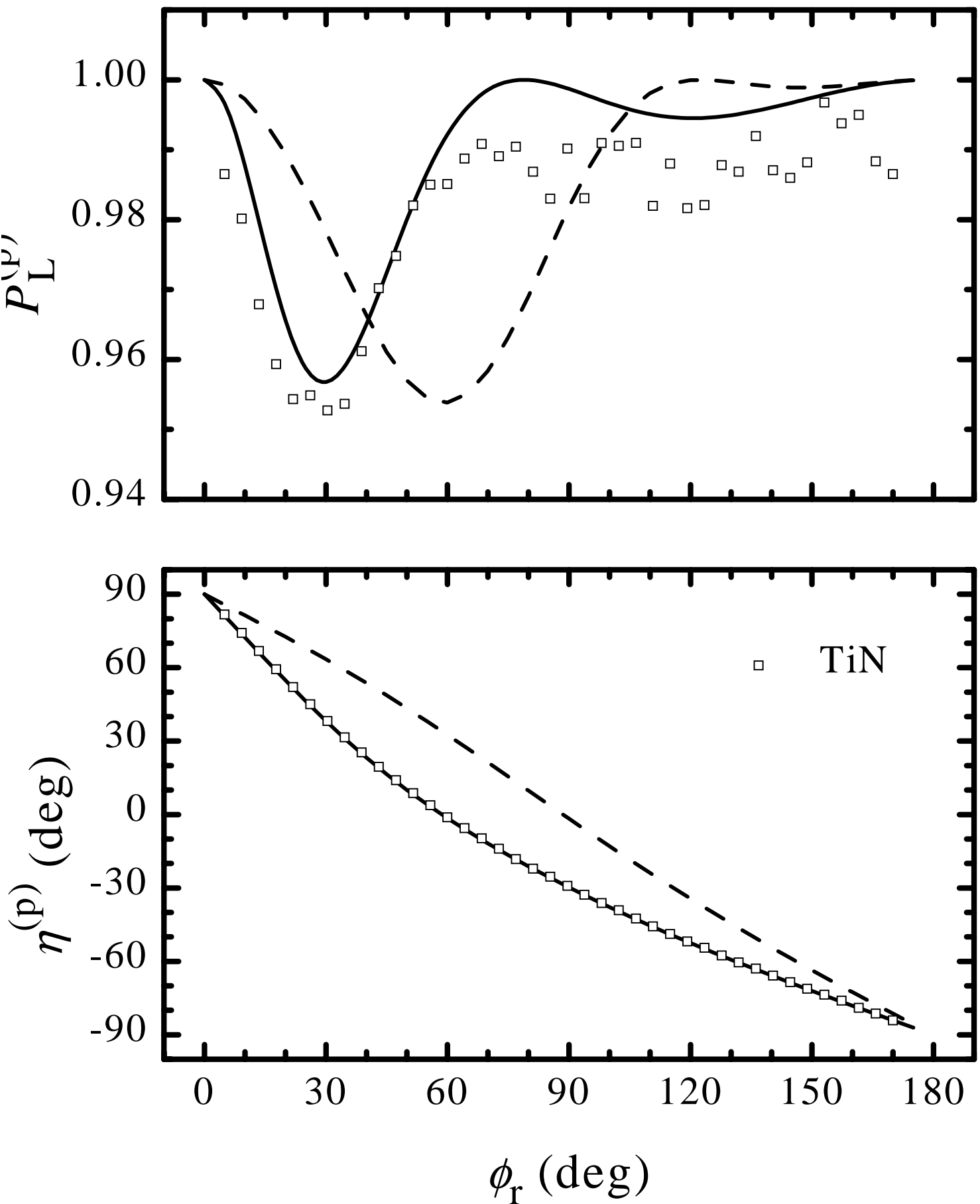
Germer and Asmail, Figure 4

Germer and Asmail, Figure 6